



Contents lists available at [SciVerse ScienceDirect](http://SciVerse.ScienceDirect.com)

## Journal of Neuroscience Methods

journal homepage: [www.elsevier.com/locate/jneumeth](http://www.elsevier.com/locate/jneumeth)



# Oversampling method to extract excitatory and inhibitory conductances from single-trial membrane potential recordings

Claude Bédard, Sebastien Béhuret, Charlotte Deleuze, Thierry Bal, Alain Destexhe\*

Unité de Neurosciences, Information et Complexité (UNIC), CNRS, 91198 Gif-sur-Yvette, France

### ARTICLE INFO

#### Article history:

Received 28 June 2011

Received in revised form 6 September 2011

Accepted 13 September 2011

### ABSTRACT

Variations of excitatory and inhibitory conductances determine the membrane potential ( $V_m$ ) activity of neurons, as well as their spike responses, and are thus of primary importance. Methods to estimate these conductances require clamping the cell at several different levels of  $V_m$ , thus making it impossible to estimate conductances from “single trial”  $V_m$  recordings. We present here a new method that allows extracting estimates of the time course excitatory and inhibitory conductances from single-trace  $V_m$  recordings. This method is based on oversampling of the  $V_m$ . We test the method numerically using models of increasing complexity. Finally, the method is evaluated using controlled conductance injection in cortical neurons *in vitro* using the dynamic-clamp technique. This conductance extraction method should be very useful for future *in vivo* applications.

© 2011 Elsevier B.V. All rights reserved.

## 1. Introduction

Neocortical neurons recorded intracellularly *in vivo* are subjected to an intense fluctuating synaptic bombardment (Azouz and Gray, 1999; Paré et al., 1998) suggesting that networks operate in a “high-conductance state” (reviewed in Destexhe et al., 2003). This synaptic conductance noise instantaneously shapes the membrane potential ( $V_m$ ) and the integrative properties of the neurons and contains information about the activity of the network. In order to access this information from intracellular recordings, several methods have been proposed to measure conductances from the  $V_m$  activity of neurons. One family of methods consists of building current–voltage relations from repeated trials in voltage clamp or current clamp, and estimating conductances from the slope of these relationships (Borg-Graham et al., 1998; Wehr and Zador, 2003; Wilentz and Contreras, 2005; reviewed in Monier et al., 2008). Another approach is statistical, and consists of estimating the statistics of conductances (such as their mean value and variance) from the  $V_m$  distribution (Rudolph et al., 2004). This method was successfully applied to estimate excitatory and inhibitory conductances in awake and naturally sleeping animals (Rudolph et al., 2007). However, all of these methods require analyzing the membrane potential at several levels (obtained by constant repetitive current injection in either voltage- or current clamp) and often relies on the averaging of several trials and thus cannot be used to estimate instantaneous variations of conductances.

More recently, a new approach was proposed to estimate conductances from single trials of  $V_m$  activity (Pospischil et al., 2009a). This method consisted of a maximum likelihood estimation of the “most likely” conductance values underlying a given voltage trace. This method could successfully estimate the mean and variance of excitatory and inhibitory synaptic conductances from single  $V_m$  traces. However, one drawback is that only estimates of the statistics of conductances are possible, but not the full time course of the conductances. Another drawback is that  $V_m$  recordings of sufficient duration and stationarity must be used to accumulate sufficient statistics for the method to provide reliable estimates (reviewed in Piwkowska et al., 2008; Pospischil et al., 2009b).

In the present paper, we propose a method to estimate the full time course of conductances from single  $V_m$  traces. The principle of our method is that if the  $V_m$  is oversampled compared to the conductances, then the supplementary information provided by this oversampling enables one to extract several variables from a single measurement. We outline the method theoretically, test it numerically in models of increasing complexity, and finally in cortical neurons *in vitro*.

## 2. Methods

### 2.1. General formulation

We first formulate the problem in a general form. The electrical circuit equivalent to the membrane is shown in Fig. 1A. This circuit is equivalent to a simpler circuit shown in Fig. 1B, where all conductances have been lumped into a single equivalent conductance

\* Corresponding author. Tel.: +33 1 69 82 34 35; fax: +33 1 69 82 34 35.  
E-mail address: [Destexhe@unic.cnrs-gif.fr](mailto:Destexhe@unic.cnrs-gif.fr) (A. Destexhe).

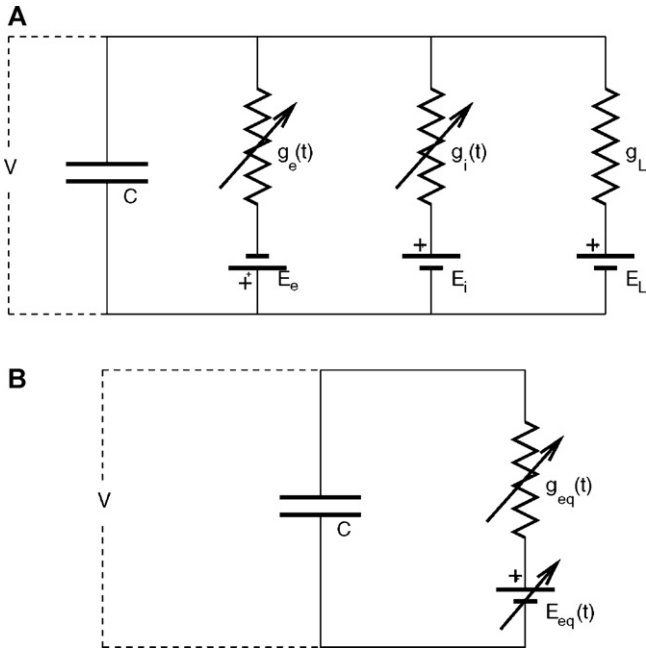


**Fig. 1.** Equivalent electrical circuits of the conductance-based models considered where the inside of the cell is at the bottom and the outside at the top. (A) Equivalent circuit for a single-compartment neuron with two time-varying synaptic conductances, excitatory  $g_e(t)$  and inhibitory  $g_i(t)$ , with their respective reversal potentials  $E_e$  and  $E_i$ .  $C$  is the membrane capacitance and  $g_L$ ,  $E_L$  are the passive conductance and reversal potential, respectively. (B) Equivalent circuit with all conductances lumped in a single equivalent conductance  $g_{eq}$  and reversal potential  $E_{eq}$ , both of which are time-dependent (see text).

$g_{eq}$ , with its time-dependent reversal potential  $E_{eq}$ . The latter circuit corresponds to the following equation:

$$C\dot{V} = g_{eq}(t)(E_{eq}(t) - V), \quad (1)$$

where  $g_{eq} = -Cg_\alpha$  and  $E_{eq} = -g_\beta/g_\alpha$ , with  $g_\alpha = -(1/C)(g_e + g_i + g_L)$  and  $g_\beta = (1/C)(g_e E_e + g_i E_i + g_L E_L)$ .  $|g_\alpha|$  is the inverse of the instantaneous membrane time constant and  $E_{eq}$  is the instantaneous reversal potential.  $E_{eq}$  is negative when  $g_\alpha$  and  $g_\beta$  are of the same sign for subthreshold membrane potentials.

In its simplest form, Eq. (1) can be written as:

$$\dot{V} = g_\alpha(t)V + g_\beta(t), \quad (2)$$

where we call  $g_\alpha(t)$  and  $g_\beta(t)$  “preconductances”, given by:

$$\begin{pmatrix} g_\alpha(t) \\ g_\beta(t) \end{pmatrix} = \frac{1}{C} \begin{pmatrix} -1 & -1 \\ E_e & E_i \end{pmatrix} \begin{pmatrix} g_e(t) \\ g_i(t) \end{pmatrix} + \frac{1}{C} \begin{pmatrix} -g_L \\ g_L E_L \end{pmatrix}. \quad (3)$$

Any complex membrane circuit with an arbitrarily large number of conductances can be formulated under the form of Eq. (2). We will consider this form in the next sections. In the case of a membrane equation with two conductances, such as Fig. 1A, estimating the preconductances is equivalent to estimating the two synaptic conductances, according to the following change of variables:

$$\begin{pmatrix} g_e(t) \\ g_i(t) \end{pmatrix} = \frac{1}{E_e - E_i} \begin{pmatrix} E_i & 1 \\ -E_e & -1 \end{pmatrix} \begin{pmatrix} Cg_\alpha - g_L \\ Cg_\beta - g_L E_L \end{pmatrix}, \quad (4)$$

where  $E_e - E_i$  is assumed to be different from zero.

In the following, we will focus on extracting the preconductances  $g_\alpha$  and  $g_\beta$ , from the measurement of  $V$ , which is a well-defined mathematical problem.

## 2.2. Idea of the oversampling method

To extract conductances from the  $V_m$  activity, we assume that the subthreshold variations of the  $V_m$  are represented by Eqs. (2) and (3).

Supposing that  $V$  is known as a time series of  $N$  values

$$V_0, V_1, V_2, \dots, V_{N-1},$$

we can rewrite this equation in discretized form:

$$\frac{1}{\Delta t}[V_{j+1} - V_j] = g_{\alpha,j}V_j + g_{\beta,j}, \quad (5)$$

where  $V_j = V(j\Delta t)$ ,  $g_{\alpha,j} = g_\alpha(j\Delta t)$ ,  $g_{\beta,j} = g_\beta(j\Delta t)$ ,  $j=0, \dots, N-1$ .

This constitutes a set of  $N$  algebraic equations for  $t=0, \dots, (N-1)\Delta t$ . The problem is that this set has  $2N$  unknowns and is therefore not solvable in general.

To solve these equations, we make the following “oversampling” approximation: we suppose that  $g_\alpha$  and  $g_\beta$  can be represented with half the sampling frequency as that of  $V$ , which corresponds to the time series of  $N/2$  values:

$$g_{\alpha,0}, g_{\alpha,2}, g_{\alpha,4}, \dots, g_{\alpha,N-2},$$

and similarly for  $g_\beta$ . We further assume that  $g_\alpha$  and  $g_\beta$  are constant within each interval  $2\Delta t$ , which is written as:

$$g_{\alpha,2k} = g_{\alpha,2k-1}, \quad (6)$$

and similarly for  $g_\beta$ , where  $k$  is a positive integer ( $k=0, \dots, [(N/2) - 1]$ ).

Thus, we can rewrite the discretized system (Eq. (5)) as:

$$\begin{cases} \frac{1}{\Delta t}[V_{2k+1} - V_{2k}] = g_{\alpha,2k}V_{2k} + g_{\beta,2k} \\ \frac{1}{\Delta t}[V_{2k+2} - V_{2k+1}] = g_{\alpha,2k}V_{2k+1} + g_{\beta,2k} \end{cases}. \quad (7)$$

Since all values of  $V(t)$  are known, the above set constitutes a set of  $N/2$  pairs of algebraic equations with 2 unknowns,  $g_{\alpha,2k}$  and  $g_{\beta,2k}$ , and is therefore solvable. In the present example, we have calculated the conductances  $g_e$  and  $g_i$  using Eq. (4) with parameters  $E_e = 0$  mV,  $E_i = -80$  mV,  $E_L = -80$  mV and  $g_L = 10^{-4}$  S/cm<sup>2</sup>.

Although in principle this procedure may work, we can see from Fig. 2 that the extracted conductances can suffer from very large errors, even including negative values which are impossible physically. What are the origins of such errors? Can we overcome them and obtain a method to reliably estimate conductances? This is the object of the next sections.

## 2.3. Extraction of the conductances

We start from the general solution of Eq. (2), which is given by:

$$V(t) = e^{\int_{t_0}^t g_\alpha(\tau)d\tau} \left[ V(t_0) + \int_{t_0}^t g_\beta(\tau)e^{-\int_{t_0}^\tau g_\alpha(\tau')d\tau'} d\tau \right]. \quad (8)$$

We can always approximate a continuous function  $f(t)$  of class  $C^0$  by a staircase function described by

$$f_T(t) = \sum_{n=1}^N \Pi_n(t)f(n\Delta nt'),$$

where  $\Pi_n(t) = H(t - n\Delta t')[1 - H(t - (n+1)\Delta t')]$  is a window function defined by two Heaviside functions  $H$ . We can do such an

<sup>1</sup> Class  $C^0$  is the ensemble of continuous functions.

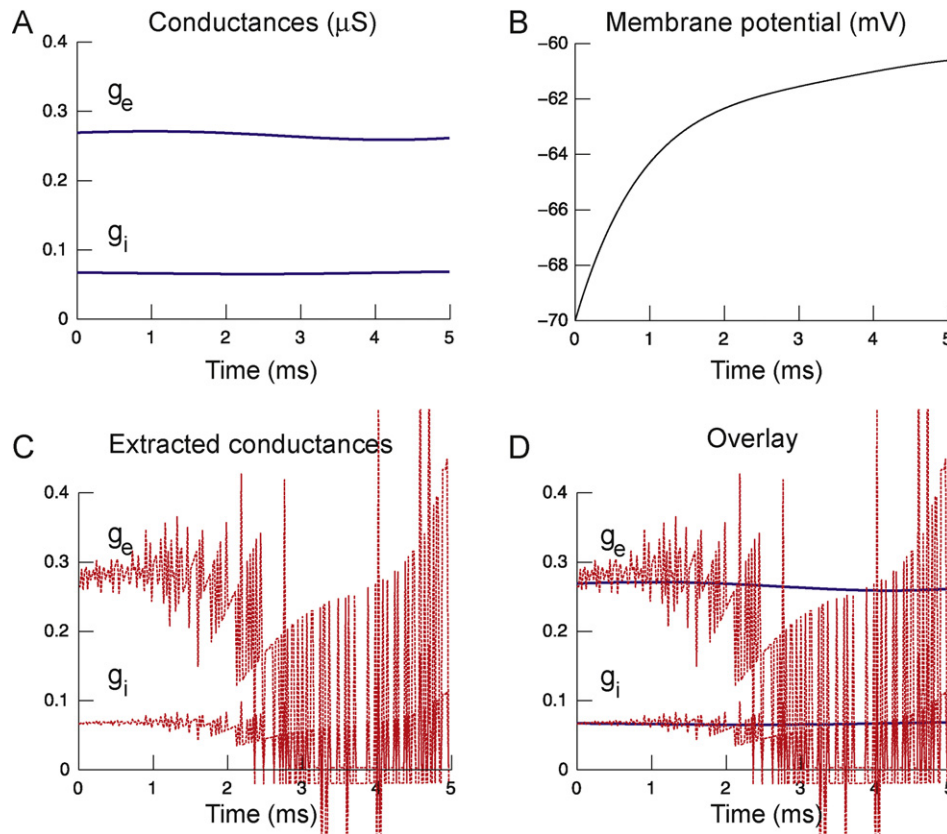


**Fig. 2.** Failure to extract conductances using a two-times oversampling of the  $V_m$ . (A) Conductances injected in a passive neuron model. (B) Resulting  $V_m$  activity. (C) Conductances extracted from the  $V_m$  activity using Eq. (7). (D) Overlay of (A) and (C).

approximation for the preconductances if they are of class  $C^0$ , which gives:

$$\begin{cases} \bar{g}_\alpha(t) = \sum_{n=1}^N \Pi_n(t) g_\alpha(n\Delta t') \\ \bar{g}_\beta(t) = \sum_{n=1}^N \Pi_n(t) g_\beta(n\Delta t') \end{cases}, \quad (9)$$

where  $\Delta t'$  is a fixed time interval. By substituting expressions (9) in the general solution (8) of Eq. (2), we obtain the following approximation for  $V$ :

$$V(t + \Delta t) = e^{g_\alpha(t+\Delta t)\Delta t'} V(t) + \frac{g_\beta(t + \Delta t')}{g_\alpha(t + \Delta t')} [e^{g_\alpha(t+\Delta t)\Delta t'} - 1], \quad (10)$$

This solution<sup>2</sup> is equivalent to considering that the preconductances  $g_\alpha$  and  $g_\beta$  are constant inside the interval  $\Delta t'$ , which is an excellent approximation when this interval is sufficiently small because the voltage error is of order 2 when the preconductance error is of order 1 (see Appendix C). If the voltage is sampled at a twice higher temporal resolution (or more) compared to the preconductances, then to insure that the solution of Eq. (2) corresponds to the measured voltage, the following condition must be satisfied:

$$\begin{cases} V(t + \Delta t) = e^{g_\alpha(t+2\Delta t)\Delta t} V(t) + \frac{g_\beta(t + 2\Delta t)}{g_\alpha(t + 2\Delta t)} [e^{g_\alpha(t+2\Delta t)\Delta t} - 1] \\ V(t + 2\Delta t) = e^{g_\alpha(t+2\Delta t)\Delta t} V(t + \Delta t) + \frac{g_\beta(t + 2\Delta t)}{g_\alpha(t + 2\Delta t)} [e^{g_\alpha(t+2\Delta t)\Delta t} - 1] \end{cases}, \quad (11)$$

<sup>2</sup> This is obtained under the assumption that the numerical solution of  $V$  between two adjacent samples satisfies the first-order differential equation with constant coefficients ( $dV/dt = g_\alpha(t_0 + \Delta t')V + g_\beta(t_0 + \Delta t')$ ), the initial condition  $V(t_0)$  and the asymptotic condition  $V(\infty) = -(g_\beta(t_0 + \Delta t'))/(g_\alpha(t_0 + \Delta t'))$ .

where  $\Delta t = \Delta t'/2$  is the time interval between two voltage samples. It follows that the preconductances are given by:

$$\begin{cases} g_\alpha(t + 2\Delta t) = \frac{1}{\Delta t} \ln \left[ \frac{V(t + 2\Delta t) - V(t + \Delta t)}{V(t + \Delta t) - V(t)} \right] \\ g_\beta(t + 2\Delta t) = \frac{V(t + 2\Delta t) - V(t)e^{g_\alpha(t+2\Delta t)\Delta t}}{e^{g_\alpha(t+2\Delta t)\Delta t} - 1} \end{cases}, \quad (12)$$

when  $(V(t + 2\Delta t) - V(t + \Delta t))/(V(t + \Delta t) - V(t)) > 0$ . However, this algorithm cannot determine the values of  $g_\alpha$  and  $g_\beta$  when we have

$$\begin{cases} (i) \quad V(t + \Delta t) - V(t) = 0 \\ (ii) \quad \frac{V(t + 2\Delta t) - V(t + \Delta t)}{V(t + \Delta t) - V(t)} < 0 \end{cases} \quad (13)$$

In the following, we will denote the points  $(t, f(t))$  which satisfy Eq. (13, i or ii) by “singular points” of the extraction algorithm.

Note that the algorithm formulated by Eq. (12) does not guarantee the uniqueness of the solution. Indeed, considering Eq. (2) as an algebraic equation, the knowledge of  $V$  does not allow in principle to extract the preconductances  $g_\alpha$  and  $g_\beta$ , because there is an infinity of couples  $(g_\alpha, g_\beta)$  which can give the same value of  $V$ . This is expressed by

$$g_\beta(t) = \frac{dV}{dt} - g_\alpha(t)V, \quad (14)$$

where for an arbitrary function  $g_\alpha(t)$ , we can calculate a function  $g_\beta(t)$  which varies according to the choice of  $g_\alpha(t)$ , while conserving the same  $V(t)$ . However, this point of view is only valid if we assume that the differential equation (2) is equivalent to an algebraic equation, which is in general not true. For example, the

continuity conditions<sup>3</sup> on  $V$  have the consequence that  $g_\alpha$  and  $g_\beta$  can be considered as constant if the interval  $\Delta t$  is sufficiently small, in which case we can write:

$$g_\beta = \frac{dV}{dt} - g_\alpha V, \quad (15)$$

where  $g_\beta$  and  $g_\alpha$  are constant. Taking the time derivative of the latter expression, we obtain

$$g_\alpha = \frac{\ddot{V}}{\dot{V}} = \frac{d}{dt} \ln \dot{V}. \quad (16)$$

The solution of these two last equations shows that we necessarily have a unique couple of possible values of  $(g_\alpha, g_\beta)$  when  $\dot{V} \neq 0$ . It follows that we have a bi-univocal correspondence between the function  $V(t)$  and the functions  $(g_\alpha(t), g_\beta(t))$  because  $\dot{V} \neq 0$  almost everywhere (except in some particular cases with constant preconductances).

In general, one can show that it is always possible to deduce from Eq. (2) an infinite number of equations by applying the time derivative operator an infinite number of times. This is the case when we approximate the preconductances by a polynomial series.<sup>4</sup> The ensemble of equations obtained define an infinite-order matrix, which inversion should allow to build a bi-univocal correspondence between  $V(t)$  and  $(g_\alpha(t), g_\beta(t))$  with respect to time (see Appendix A). Approximating these functions by polynomial series, leads to the operator  $\hat{E}_{ex}$

$$\begin{pmatrix} g_\alpha \\ g_\beta \\ \dot{g}_\alpha \\ \dot{g}_\beta \\ \vdots \end{pmatrix} = \hat{E}_{ex} \begin{pmatrix} \dot{V} \\ \ddot{V} \\ \ddot{V} \\ \ddot{V} \\ \vdots \end{pmatrix},$$

which enables extracting the preconductances from the sole knowledge of  $V(t)$ , as shown in Appendix A. Moreover, in this Appendix, we show that this algorithm is a first-order finite difference approximation of the following expression:

$$\begin{pmatrix} g_\alpha \\ g_\beta \end{pmatrix} = \frac{1}{\dot{V}} \begin{pmatrix} 0 & 1 \\ \dot{V} & -V \end{pmatrix} \begin{pmatrix} \dot{V} \\ \ddot{V} \end{pmatrix}, \quad (17)$$

which is itself a first-order approximation of the extraction operator  $\hat{E}_{ex}$  for the preconductances (see Eqs. (31) and (32) in Appendix A).

Thus, in this article, we use the first-order approximation of the extraction operator to extract the values of  $g_\alpha$  and  $g_\beta$ . In the next section, we will see how to suppress the numerous singular points generated by this extraction procedure.

## 2.4. Suppression of singular points

To remove the first two types of singular points (see Eq. (13); see Appendix A), we need one procedure to identify the singular point and another procedure to suppress them. In addition, the discretization of the system generates a third type of singular point (see Appendix B), and a fourth type of singularity can be generated by abrupt transitions in the conductances. We will successively examine these different singular point below.

<sup>3</sup> According to Eq. (2),  $V$  is necessarily continuous because  $V$  must be time derivable.

<sup>4</sup> Note that by virtue of the Weierstrass theorem, it is always possible to approximate by a polynomial suite any function which is bounded, continuous and defined over a compact interval.

### 2.4.1. Algorithm to identify singular points

The first type of singular point (Eq. (13), i) is easily identified because it occurs when the derivative of the voltage is zero (or quasi-zero), and the logarithmic time derivative of the preconductances becomes very large because we have  $(d/dt) \ln(g_\alpha) = (d/dt) \ln(d/dt) \ln \dot{V}$  (see Eq. (16)). Thus, this can be identified by calculating the logarithmic derivative of  $g_\alpha$  and  $g_\beta$  and define two thresholds  $\kappa_\alpha$  and  $\kappa_\beta$  according to:

$$\begin{cases} \frac{\Delta g_\alpha}{g_\alpha} > \kappa_\alpha \\ \frac{\Delta g_\beta}{g_\beta} > \kappa_\beta \end{cases}. \quad (18)$$

In this article, the thresholds  $\kappa_\alpha$  and  $\kappa_\beta$  will be fixed empirically. The numerical simulations and biological experiments (see Section 3) indicate that reasonable values of those parameters are around 0.1. If these parameters are too large, singular points will be missed, whereas if they are too small the singular points will tend to occur at every point. Note that a consistency check can be used to verify that the values of  $\kappa_\alpha$  and  $\kappa_\beta$  are adequate, namely to solve Eq. (2) with the extracted preconductances and compare this solution to the original function  $V(t)$ .

The second type of singular point (Eq. (13), ii) arises from the fact that the argument of the logarithm is negative,

$$\frac{V(t + 2\Delta t) - V(t + \Delta t)}{V(t + \Delta t) - V(t)} < 0,$$

in the finite difference approximation of  $g_\alpha = (d/dt) \ln(\dot{V})$  and  $g_\beta = \dot{V} - ((d/dt) \ln \dot{V})V$ . This case can be recognized either by directly testing the value of the argument, or by the fact that the value of  $g_\alpha$  becomes complex. We have considered the second option because it allows us to treat the values of  $g_\alpha$  and  $g_\beta$  identically as for the first type of singular point above.

In principle, recognizing these two types of singular points should be sufficient in a real biological signal, because the preconductances are necessarily analog and continuous in time (for example real synaptic inputs in a neuron). However, for digital signals, a third type of singular point appears (see Section 3.5 and Appendix B). To understand this, we will use a representation of preconductances using a continuous staircase representation (Eq. (9)) of the sequence of values resulting from the digitization.

Each function  $\square_n$  in Eq. (9) will generate a Dirac delta function in the second derivative of the voltage (see Eq. (2)). From the relations  $\dot{V} = g_\alpha \dot{V}$  and  $\dot{V} = g_\alpha V + g_\beta$  one can easily see that each significant numeric variation of  $g_e$  and  $g_i$  will determine a singularity in the extraction of the preconductances  $g_\alpha$  and  $g_\beta$ . Thus, extracting digitized conductances will cause numerous singular points of this third type, as indeed seen in Fig. 2. To solve this problem, the sampling frequency of the voltage must be at least  $4 = 3 + 1$  times larger than that of the conductances, because 1 point is needed to suppress the third-type of singular point, and more points are needed to extract the preconductances values. A minimum of 3 voltage points ( $V(t)$ ,  $V(t + \Delta t)$ ,  $V(t + 2\Delta t)$ ) (see Eq. (12)) with no singularity is needed to correctly apply the extraction algorithm. Fortunately, one can identify Type 3 singularities using the same algorithm as for Type 1 and Type 2.

Finally, the fourth type of singularity occurs when there are real abrupt transitions in the conductances. For example, the sudden opening of ion channels can generate very sharp transitions, the rise time of some synaptic currents can be very fast, etc. Such a situation will correspond mathematically to have additional Heaviside functions due to the abrupt variations of conductance, in addition to the Heaviside functions due to the digitization. This additional Heaviside function will be responsible for a 4th type of singularity.

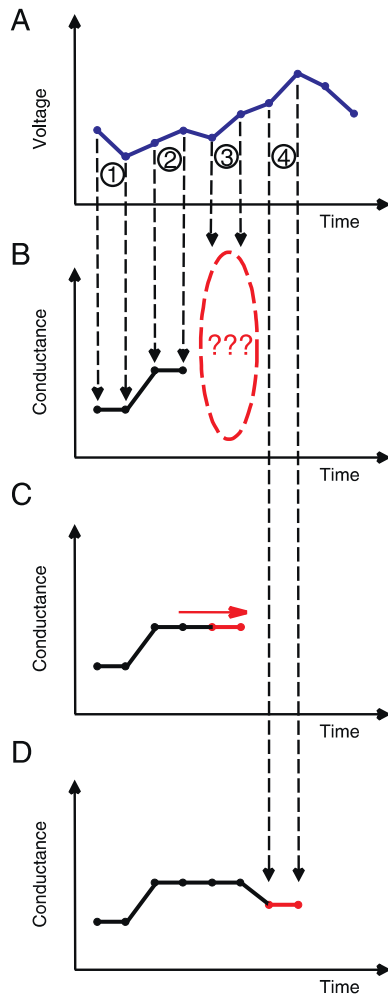


**Fig. 3.** Scheme to illustrate the suppression of singular points in the extraction procedure. The algorithm to extract the digitized preconductances can generate four types of singularities (see text). The figure illustrates the case where the sampling frequency of  $V$  (A) is twice that of preconductances and conductances (B). The extraction proceeds by evaluating the conductances from successive couple of points of  $V$  (1 and 2 in A), until a singularity occurs (couple 3 in A; dashed circle in B). Once such singularity is identified, the corresponding conductance points are duplicated from the values extracted in the preceding step (C, arrow). Next, the extraction proceeds with the next couple of points (4 in A and D). Note that the same procedure can be applied in the case the conductance is oversampled with a factor larger than two. The average over some time window preceding the singularity can also be used instead of duplicating the values (see text).

Here again, they can be identified using the same procedure as for the other types of singularities.

#### 2.4.2. Algorithm to suppress singular points

As illustrated in Fig. 3, the singular points are suppressed by duplicating the extracted values obtained at the preceding step. Note that instead of duplicating the preceding values, it is also possible to use an average over some time window. The latter procedure will be used to extract conductances from experimental data (see Section 3.5) because it is more robust to the presence of noise in the recording. In such a case, a window of 20 successive points (immediately preceding the singularity) was found to provide robust extraction results (see below).

#### 2.5. Biological experiments

All research procedures concerning the experimental animals and their care adhered to the guidelines of the American

Neuroscience Association, to the European Council Directive 86/609/EEC and to European Treaties series no. 123, and were also approved by the local ethics committee “Ile-de-France Sud” (certificate no. 05-019).

*In vitro* experiments were performed on 300  $\mu\text{m}$  thick horizontal slices from somatosensory cortex of P15 Swiss mice. Animals were anesthetized with 3% isoflurane, decapitated, and the brains rapidly removed and immersed in a ice-cold slicing solution containing (in mM) 234 sucrose, 2.5 KCl, 10  $\text{MgSO}_4$ , 1.25  $\text{NaH}_2\text{PO}_4$ , 0.5  $\text{CaCl}_2$ , 26  $\text{NaHCO}_3$ , and 10 dextrose and equilibrated with 95% $\text{O}_2$ /5% $\text{CO}_2$  to a final pH of 7.4. The slices were incubated initially at 32  $^\circ\text{C}$  for 1 h and then at room temperature in artificial cerebrospinal fluid (ACSF) containing (in mM): 126 NaCl, 2.5 KCl, 2  $\text{MgCl}_2$ , 1.25  $\text{NaH}_2\text{PO}_4$ , 2  $\text{CaCl}_2$ , 26  $\text{NaHCO}_3$ , and 10 dextrose equilibrated with 95% $\text{O}_2$ /5% $\text{CO}_2$  to a final pH of 7.4. Slices were then transferred to a recording chamber and maintained at 32  $^\circ\text{C}$  with a continuous ACSF bath perfusion. Experiments were performed in the presence of the ionotropic glutamate receptor blockers DL-(–)-2-amino-5-phosphopentanoic acid (DL-AP5, 100  $\mu\text{M}$ ) and 6,7-dinitroquinoxaline-2,3-dione (DNQX, 10  $\mu\text{M}$ ), and the GABA<sub>A</sub> receptor antagonist gabazine (10  $\mu\text{M}$ ). All drugs were obtained from Tocris Cookson (Ellisville, MO).

We performed patch-clamp whole-cell recordings from visually identified cells in layer V of sensorimotor neocortex using infrared video-microscopy (Axioskop Microscope, Carl Zeiss, Germany). Electrodes (tip resistance 2–3  $\text{M}\Omega$ ) were filled with an intracellular solution containing (in mM): 135 Kgluconate, 10 HEPES, 1 EGTA, 5  $\text{MgCl}_2$ , 0.1  $\text{CaCl}_2$ , 4  $\text{Na}_2\text{-ATP}$ , pH 7.3, 290 mOsm. A liquid junction potential of +10 mV was systematically corrected before recording. A Multiclamp 700B amplifier (Axon Instruments) was used for  $V_m$  recording and current injection in the current clamp mode via a NI-PCIE-6251 acquisition board (Texas Instruments) coupled to both a home-made software (G. Sadoc, ELPHY, CNRS-UNIC) and a real time version (Sadoc et al., 2009) of the NEURON simulator (Hines and Carnevale, 1997) for dynamic clamp. RT-NEURON ran in the INtime kernel (Tenasys) combining hard real-time control with standard Windows operating systems without requiring additional hardware.

The dynamic-clamp technique (Robinson and Kawai, 1993; Sharp et al., 1993) was used to inject computer-generated conductances in cortical neurons *in vitro* at a sampling frequency of 5000 Hz. Dynamic-clamp experiments were run using the RT-NEURON environment as described previously (Sadoc et al., 2009). In these experiments, the injected current  $I(t)$  was determined from the conductances  $g_e(t)$  and  $g_i(t)$  as well as from the difference between the recorded membrane voltage  $V$  and the respective reversal potentials:

$$I(t) = -g_e(t)(V - E_e) - g_i(t)(V - E_i). \quad (19)$$

The passive parameters of the recorded cells,  $C$ ,  $g_L$  and  $E_L$  were estimated as follows. Assuming that the cell is equivalent to a single-compartment, the injected current equals

$$I(t) = C \frac{dV}{dt} + g_L(V - E_L). \quad (20)$$

To estimate passive parameters, one first computes the impedance  $|Z_\omega| = |(V_\omega)/(I_\omega^*)|$ , where  $V_\omega$  and  $I_\omega^*$  are the Fourier transforms of  $V$  and  $I^* = I + k$ , respectively. We took advantage of the fact that the slope of  $|Z_\omega|$  is zero at low frequencies when  $k = g_L E_L$ , because we have

$$|Z_\omega| = \left| \frac{V_\omega}{I_\omega^*} \right| = \frac{1}{g_L + i\omega C},$$

if  $k = g_L E_L$ . Thus, one can fit  $|Z_\omega|$  against the experimental data because in dynamic-clamp experiments, one has access to both  $I(t)$

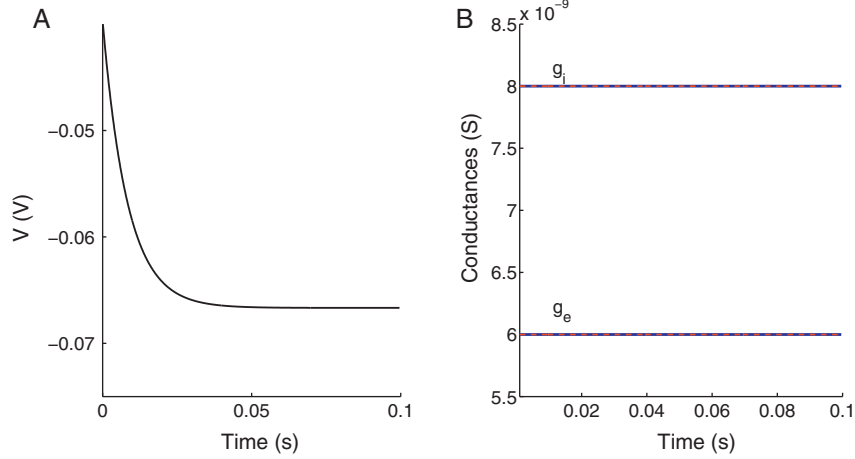


**Fig. 4.** Extraction of constant conductances. (A) Values of  $V$  as a function of time when  $g_e$  and  $g_i$  are constant. (B) Original conductances (blue) and extracted conductances (red, dashed). These conductances are perfectly superimposed. Note that there is no singularity in this particular case. Parameters:  $E_e = 0$  mV,  $E_i = -70$  mV,  $E_L = -80$  mV,  $g_L = 28$  nS and  $C = 0.35$  nF. (For interpretation of the references to color in this figure legend, the reader is referred to the web version of this article.)

and  $V(t)$  to estimate the parameters  $g_L$  and  $C$ . The parameter  $E_L$  is given by  $k/g_L$  and is the resting membrane potential of the cell.

### 3. Results

We start by examining the extraction of conductances from the  $V_m$  activity using cases of increasing complexity, using numerical simulations, and then we test the extraction method in real neurons using dynamic-clamp experiments.

#### 3.1. Simplest case: constant conductances

The simplest example is when there is no time dependency in the conductances, in which case there is no singularity. As shown in Fig. 4, the conductances are perfectly well extracted in this case. Note that if Eq. (2) is considered as an algebraic equation may give the false impression that there is an infinity of combinations of  $(g_\alpha, g_\beta)$  which gives the same  $V$ . However, as we showed in Section 2 (see also Appendix A), there is an extraction operator which guarantees the uniqueness of the solution  $(g_\alpha, g_\beta)$ .

Note that this example is very different from Fig. 2, in which the conductances were quasi-constant. In that case, even small variations of the conductances can cause singular points, as we will also see below.

#### 3.2. Smooth periodic variations of conductances

In this section, we use simple periodic functions (sine and cosine) to illustrate the singular points with digitized conductances. We use the following periodic functions:

$$\begin{aligned} G_e(t) &= g_e^a \left[ \cos\left(\frac{t}{100}\right) + \left(\frac{7}{6}\right) \right] \\ G_i(t) &= g_i^a \left[ \sin\left(\frac{t}{100}\right) + \left(\frac{9}{8}\right) \right] \end{aligned} \quad (21)$$

sampled at a frequency of  $f_e = 2.5$  kHz and by using  $g_e^a = 6$  nS and  $g_i^a = 8$  nS. Using the continuous staircase expression for the conductances gives:

$$\begin{aligned} g_e(t) &= \sum_{n=1}^N g_e^a \Gamma_n(t) \left[ \cos\left(\frac{n\Delta}{100}\right) + \frac{7}{6} \right] \\ g_i(t) &= \sum_{i=1}^N g_i^a \Gamma_n(t) \left[ \sin\left(\frac{n\Delta}{100}\right) + \frac{9}{8} \right] \end{aligned}, \quad (22)$$

where  $\Delta = 1/f_e$  and  $\Gamma_n(t) = H(t - n\Delta)[1 - H(t - (n+1)\Delta)]$ .

Applying Eq. (3), we obtain:

$$\begin{aligned} g_\alpha(t) &= -\frac{1}{C} \sum_{n=1}^N \Gamma_n(t) \left[ g_e^a \left[ \cos\left(\frac{n\Delta}{100}\right) + \frac{7}{6} \right] + g_i^a \left[ \sin\left(\frac{n\Delta}{100}\right) + \frac{9}{8} \right] + g_L \right] \\ g_\beta(t) &= \frac{1}{C} \sum_{n=1}^N \Gamma_n(t) \left[ E_i g_i^a \left[ \sin\left(\frac{n\Delta}{100}\right) + 1.16 \right] + g_L E_L \right] \end{aligned} \quad (23)$$

Here,  $g_L = 28$  nS,  $E_L = -80$  mV,  $E_e = 0$  mV,  $E_i = -70$  mV,  $C = 0.35$  nF and  $I(t) = 0$ .

To calculate the solution of Eq. (2), we used a sampling frequency of 10 kHz for  $V$ , which is four times larger than that of conductances. Using Eq. (10), we obtain the following recurrence relation:

$$V(t + \Delta') = e^{g_\alpha(t+\Delta')\Delta'} V(t) + \frac{g_\beta(t + \Delta t')}{g_\alpha(t + \Delta')} [e^{g_\alpha(t+\Delta')\Delta'} - 1], \quad (24)$$

where  $\Delta'$  is 4 times smaller than  $\Delta$ .

This numerical solution of equation  $\dot{V} = g_\alpha V + g_\beta$  is such that  $\dot{g}_\alpha = 0$  and  $\dot{g}_\beta = 0$  when there is no singular point of Type 3. In such a case, we can apply the extraction algorithm presented in Section 2 (see Eq. (12)).

The results presented in Fig. 5 show that the extraction gives values consistent with the theory (see Appendix B). The algorithm works very well in this case, when singular points are removed.

#### 3.3. Smooth aperiodic conductance variations

In this section, we consider a more complex model consisting of smooth conductance variations following temporally irregular and aperiodic dynamics. We chose the Rossler (1976) model, which consists of three coupled first-order differential equations displaying deterministic chaos. The conductances  $g_e$  and  $g_i$  are given by:

$$\begin{aligned} \dot{g}_e &= -g_i - z \\ \dot{g}_i &= g_e + a g_i \\ \dot{z} &= b + z(g_e - c) \end{aligned}, \quad (25)$$

where  $E_e = 0$  mV,  $E_i = -75$  mV,  $E_L = -80$  mV,  $g_L = 1.56$  nS and  $C = 0.346$  nF. The model is considered in the parameter region displaying deterministic chaos ( $a = 0.38$ ,  $b = 0.30$ ,  $c = 4.5$ ).

As shown in Fig. 6, the extraction procedure gives excellent results in this case when singularities are removed.

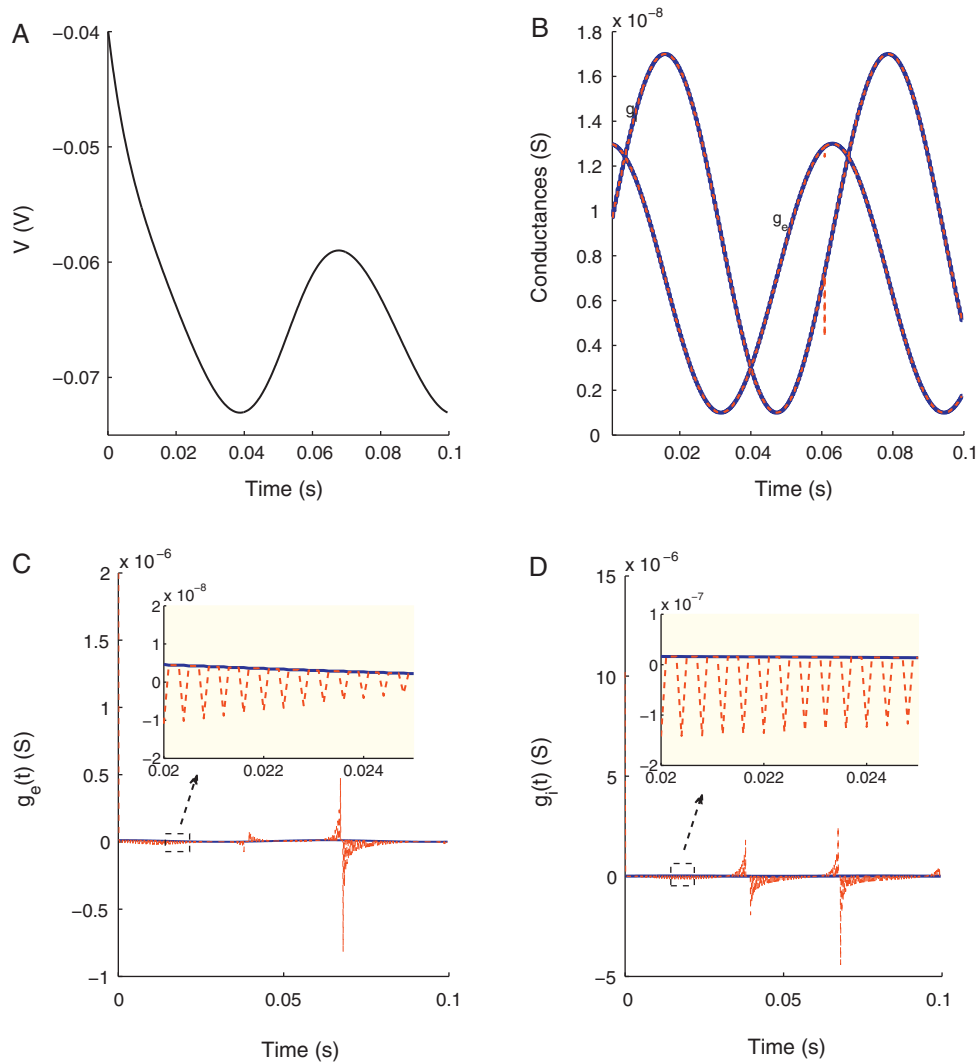


**Fig. 5.** Extraction of smooth periodic conductances. (A) Membrane potential generated by periodic conductances given by  $g_e^d(\cos(t/100) + (7/6))$  and  $g_i^d(\sin((t/100) + (9/8)))$  where  $g_e^d = 6$  nS and  $g_i^d = 8$  nS. Other model parameters were  $E_e = 0$  mV,  $E_i = -70$  mV,  $E_L = -80$  mV,  $g_L = 28$  nS and  $C = 0.35$  nF. (B) Results of the extraction procedure. The theoretical conductances injected in the model are shown in blue, and the conductances extracted from the  $V_m$  are shown with dashed red lines, after having removed the singular points ( $\kappa_\alpha = 0.1$  and  $\kappa_\beta = 0.1$ ). (C and D) Results of the extraction when singular points are not removed. Insets: details at higher resolution. Note that in between singularities (sharp deflections in red), the extraction algorithm gives correct conductance estimates, except for values around 0.06 s. (For interpretation of the references to color in this figure legend, the reader is referred to the web version of this article.)

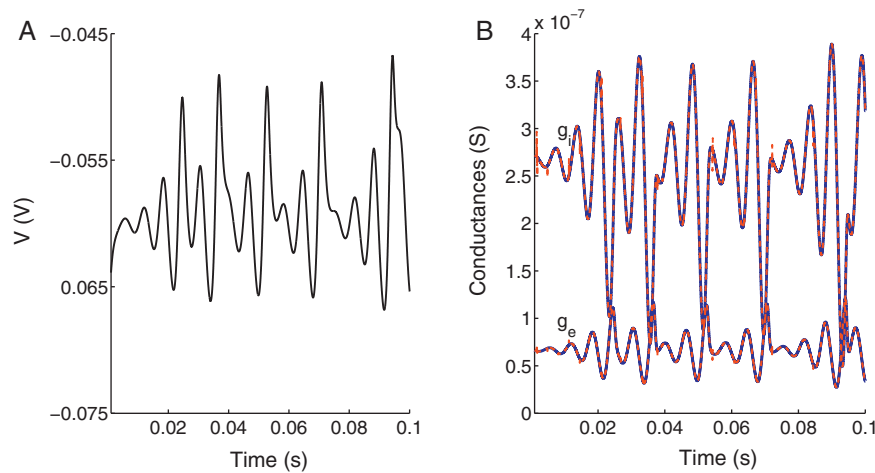


**Fig. 6.** Extraction of smooth aperiodic patterns of conductances. (A) Time course of the membrane potential  $V$  of a model subject to aperiodic variations of  $g_e$  and  $g_i$  conductances described by the Rossler model (see text). (B) Results of the extraction procedure. The conductances injected in the model are shown with blue curves, while the conductances extracted from  $V$  are drawn as dashed red curves. The values of the thresholds were of  $\kappa_\alpha = 0.1$  and  $\kappa_\beta = 0.2$ . (For interpretation of the references to color in this figure legend, the reader is referred to the web version of this article.)

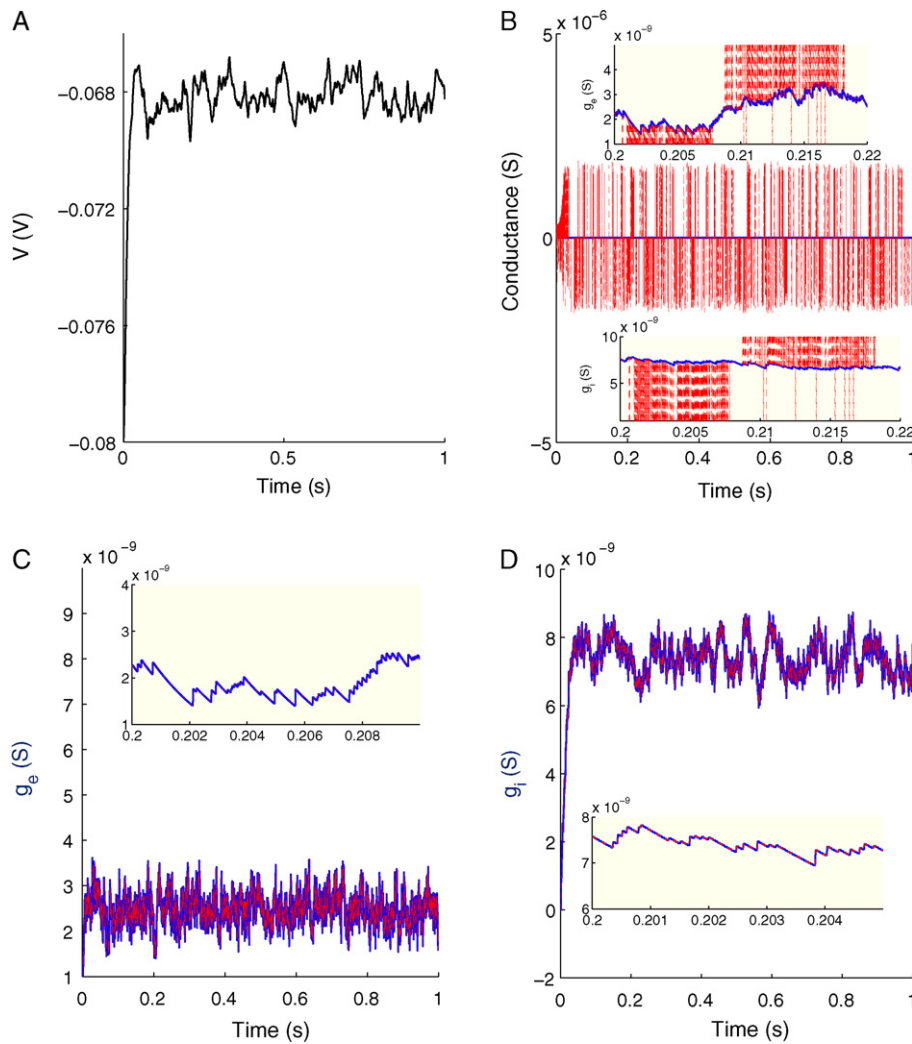


**Fig. 7.** Extraction of stochastic synaptic conductances. (A) Membrane potential  $V$  generated by stochastic excitatory and inhibitory conductances (sampling of  $V$  was 4 times higher than that of conductances). Model parameters:  $E_e = 0$  mV,  $E_i = -70$  mV,  $E_L = -80$  mV,  $g_L = 28$  nS and  $C = 0.35$  nF. (B) Results of the extraction procedure, including the removal of Type 1, 2, 3, 4 singularities with  $\kappa_\alpha = 0.1$  and  $\kappa_\beta = 0.1$ . The singularities that appear are due to abrupt variations of conductances. (C and D) Extracted conductances after removal of singularities (the insets show details of at higher temporal resolution). In (B–D), the theoretical conductances are drawn in blue, while the extracted conductances are drawn as dashed red curves. (For interpretation of the references to color in this figure legend, the reader is referred to the web version of this article.)

### 3.4. Stochastic conductance variations

In this section, we consider the most complex case of synaptic conductance varying stochastically. In this example, the conductances are given by a shot-noise model, and consist of:

$$\begin{aligned} \dot{g}_e &= \sum_i H(t - t_i) \exp\left[\frac{-(t - t_i)}{\tau_e}\right] \\ \dot{g}_i &= \sum_j H(t - t_j) \exp\left[\frac{-(t - t_j)}{\tau_i}\right], \end{aligned} \quad (26)$$

where  $t_i$  and  $t_j$  are the times of presynaptic spikes for excitatory and inhibitory synapses; these times are distributed randomly in time, according to Poisson processes.

The extraction procedure in this case is shown in Fig. 7. In such a case of stochastically varying conductances, the Heaviside functions  $H$  in Eq. (26) will cause Type 4 singularities, in addition to the other singularities, as shown in Fig. 7B. Removing these singularities leads to extracted conductances in excellent agreement with the conductances injected in the model (Fig. 7C and D).

### 3.5. Injection of artificial synaptic conductances in vitro

In this last section, we consider another stringent test, the injection of stochastic conductances in real cortical neurons. We used the same model of conductances varying as a shot-noise as in the previous section, but injected in cortical neurons using the dynamic-clamp technique (see Section 2). A critical aspect is to correctly estimate the passive parameters of the cells. To this end, we have used a procedure based on the Fourier transforms of  $V$  and  $I$ , as explained in Section 2. A total of 3 cells were recorded.

Fig. 8 illustrates the results of the extraction method applied to a dynamic-clamp experiment. One can see that the conductances extracted from the  $V_m$  activity (red) are in very good agreement with the injected conductances (blue). However, this result was critically dependent on a number of adjustments.

First, an oversampling factor of 6 had to be used in this experiment to correctly remove the numerous singularities. Oversampling factors of 2 and 4 were tested, but produced too many singular points.

Second, because of the presence of instrumental noise, the procedure for suppressing singularities had to rely on a moving average of 20 data points immediately preceding the singularity

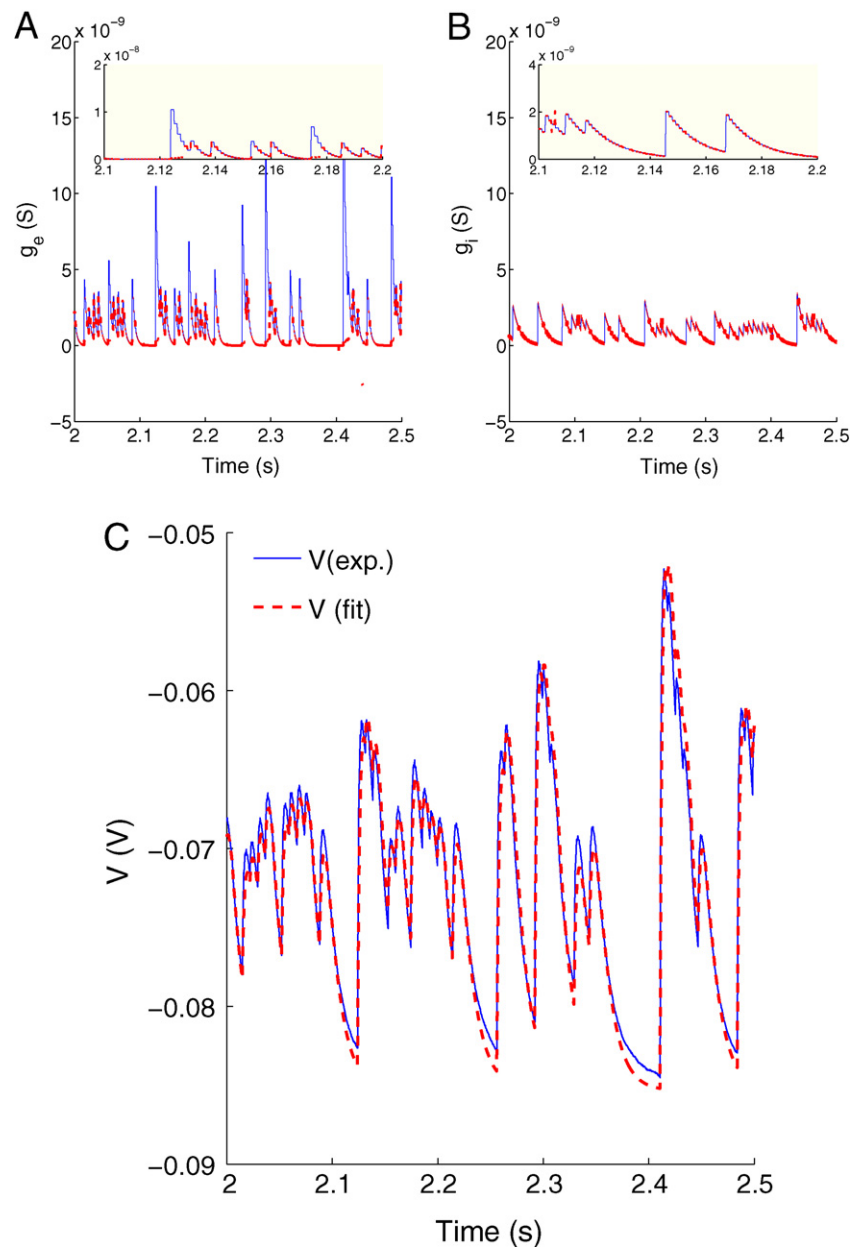


**Fig. 8.** Extraction of conductances in cortical neurons *in vitro*. Excitatory (A) and inhibitory (B) conductances injected in a neuron in mouse visual cortex slices using the dynamic-clamp technique (blue curves). The conductances extracted from the recorded  $V_m$  activity are shown in red, and the insets show details at higher temporal resolution. The parameters of the conductances were  $E_e = 0$ ,  $E_i = -85$  mV, and the estimated passive parameters of the cell shown here were  $E_L = -85.41$  mV,  $C = 0.09$  nF and  $g_L = 6$  nS. The sampling frequency of  $V$  was 5 kHz and was 6 times larger than the conductances  $g_e$  and  $g_i$ . (C) The temporal variations of the conductances were produced by a shot-noise model (see Section 3.4). Comparison between the recorded  $V$  following conductance injection (red) to the  $V$  predicted by a single-compartment model (blue) with the same passive properties of the cells, and with the extracted conductances. (For interpretation of the references to color in this figure legend, the reader is referred to the web version of this article.)

(see Section 2). This procedure was used because the presence of noise in the recording of  $V$  creates instabilities in the extraction of the preconductances. We tested 5, 10, 20 points and acceptable results were obtained with 20 points. Note that this factor applies to the  $V_m$  sampling, and means that for some segments of data, the temporal precision of the extracted conductances was 20 times less than that of the  $V_m$ . Another possibility – not tested here – is to use techniques for removing noise from the  $V_m$  activity.

Using these settings, some of the fast transient conductances of  $g_e$  were not correctly captured (see Fig. 8A and insets). This error is presumably due to the moving average of 20 points, which produces an effective “filtering” of the data and thus removes fast transients. Due to this averaging, the temporal resolution

of the conductances is about 20 times less than the  $V_m$  activity. In the example shown in Fig. 8, the temporal resolution on  $V$  was 0.2 ms, but the resolution on conductances was 4 ms. Nevertheless, even with this down-sampling factor, the extraction provides estimates of conductance which are of very reasonable accuracy.

#### 4. Discussion

In this paper, we have shown theoretically and experimentally that it is possible to extract conductances from single traces of  $V_m$  recordings, under some conditions. First, the  $V_m$  must be

subthreshold, so that the equation for  $V$  remains linear, which is a prerequisite for the present method to apply. If the  $V_m$  trace contains action potentials, they should be removed because the underlying membrane equation is nonlinear, in which case the present theory does not hold. The second condition is that an oversampling factor is required between the  $V_m$  and the conductances to extract. This is also a requisite of the present method. The third condition is to obtain procedures to remove the singular points which will necessarily appear in the extraction procedure. We have illustrated the application of these principles using numerical simulations of increasing complexity, and tested it on cortical neurons *in vitro* using the dynamic-clamp technique.

The principle of the extraction method is that there is a unique correspondence between the oversampled membrane potential and two variables, which we call “preconductances” (see definition in Section 2). The uniqueness of preconductances can be demonstrated formally (see Appendix A). In a second step, the conductances are extracted from the preconductances. In simple cases with two voltage-independent conductances (excitatory and inhibitory), there is also a unique correspondence between conductances and preconductances, and thus uniqueness is also guaranteed for the conductances. In principle, this method can be applied to extract more than two conductances, but in this case uniqueness is guaranteed for the preconductances, but not necessarily for the conductances. This extension of the method should be considered in future work.

It is important to note that in all simulations done here, as well as in the dynamic-clamp experiments, we have assumed that the cell is well described by a single compartment RC circuit. Here again, the exact model only concerns the conversion from preconductances to conductances. All simulations were done with this standard RC model, and of course the extraction yielded the expected result. However, for dynamic-clamp experiments, we have shown that there is a significant error as not all fast transients were captured by the extraction method. Part of this deviation may be attributable to the “filtering” which is due to the time-averaging (20 data points in Fig. 8) which necessarily removes some of the fast components of conductances. It may also be due to the fact that the recorded cell is more complex than a simple RC circuit. Like somatic voltage-clamp, the present method extracts the conductances as “visible” from the recording site (the soma in most cases), which may be different from the conductances present in dendrites. Another limitation is that the  $V_m$  recording must be at the highest sampling frequency as possible, to enable removing the singularities. Besides these limitations, we can consider that the extracted conductances are of very reasonable accuracy.

To date, no other method has been proposed to extract the full time course of conductances from single traces of membrane potential activity, but several alternatives exist. For example, one can extract excitatory and inhibitory conductances from  $V_m$  activity by building current–voltage relations with repeated trials (for a review, see Monier et al., 2008). However, this approach requires repeated trials at different levels of DC current injection, so it only can be applied to specific responses to well-timed stimuli, but not to spontaneous activity. Another approach was proposed to estimate statistical properties of excitatory and inhibitory conductances from single  $V_m$  traces (Pospisil et al., 2009a). This approach provides estimates of the mean and variances of synaptic conductances, but not of the full time course of conductances, as proposed by the present method.

The present method should be applied to intracellular recordings *in vivo* in the future, as well as compared to conductances estimated by other methods. For example, by using classical conductance estimates from repeated trials (Monier et al., 2008), it should be possible to analyze the individual traces with the present

method, and obtain the conductance time courses of individual trials, which average value should match the former estimates. This is another possible test and extension of the present work.

## Acknowledgments

This research study was supported by the CNRS, Agence Nationale de la Recherche (ANR HR-Cortex, Complex-V1) and the European Community (FET grants FACETS FP6-015879, BrainScales FP7-269921). A MATLAB (Mathworks, Inc.) program code that runs the method presented here and reproduces some of the figures of the present paper, is available at our web site <http://cns.iaf.cnrs-gif.fr>: <http://cns.iaf.cnrs-gif.fr/files/extraction-demo.zip> and at the ModelDB database: <http://senselab.med.yale.edu/senselab/ModelDB>.

## Appendix A. Uniqueness of extracted preconductances

In this appendix, we show that there is a bi-univocal correspondence between the membrane potential  $V(t)$  and the preconductances  $(g_\alpha(t), g_\beta(t))$  in a single-compartment model neuron (see Fig. 1). We show that there is a unique operator  $\hat{E}_{ex}$  which allows extracting the preconductances  $g_\alpha$  and  $g_\beta$ .

To demonstrate this, we express the functions as polynomials, and we use the Weierstrass theorem to demonstrate uniqueness. On a topological point of view, the approximation of a continuous function  $f$  by a polynomial sequence is equivalent to use a sequence of staircase functions (see Eq. (9)) when these functions are in  $L^2$ . Thus, demonstrating the uniqueness of the extraction operator is also valid for the ensemble of all staircase functions. By virtue of the triangular inequality, we can write:

$$\|f - f_n^\perp\|_{L^2} = \|f - P_n + P_n + f^\perp\|_{L^2} \leq \|f - P_n\|_{L^2} + \|P_n - f_n^\perp\|_{L^2} \quad (27)$$

and

$$\|f - P_m\|_{L^2} = \|f - P_m + f_m^\perp - f_n^\perp\|_{L^2} \leq \|f - f_m^\perp\|_{L^2} + \|P_m - f_n^\perp\|_{L^2} \quad (28)$$

such that the open ensembles defined by the two types of sequence are homeomorphic, because in  $L^2$ , we can approximate to any degree of accuracy any staircase function by a polynomial sequence, and *vice versa*. On a theoretical point of view, it is more interesting to work with polynomial sequences than with staircase functions, because the former enables using the derivative operator, which will allow us here to analytically determine the extraction operator. Staircase functions are more practical for numerical approximations.

The **Weierstrass theorem** (see Rudin, 1976) demonstrates that if we have a real and continuous function  $f$ , defined over the real interval  $[a, b]$ , then there is a polynomial sequence  $(P_n)$  which uniformly converges towards  $f$  on  $[a, b]$ . It follows that it is always possible to build a mathematical model  $M_w$  (Weierstrass model) of the preconductances  $g_\alpha$  and  $g_\beta$ , with any required accuracy, such that preconductances can be represented as a time-dependent polynomial. Because the general solution of Eq. (2) is such that  $V$  is holomorphic when preconductances are holomorphic, we can say that the membrane potential is holomorphic when the preconductances are represented by a Weierstrass model.<sup>5</sup>

<sup>5</sup> Because a polynomial is holomorphic.

Applying the operator ( $d/dt$ ) on Eq. (2) an infinite number of times and writing the ensemble of solutions in matrix form, gives:

$$\begin{pmatrix} \hat{d}^1 V \\ \hat{d}^2 V \\ \hat{d}^3 V \\ \hat{d}^4 V \\ \vdots \end{pmatrix} = \begin{pmatrix} V & 1 & 0 & 0 & 0 & 0 & 0 & 0 & 0 & \dots \\ \hat{d}^1 V & 0 & V & 1 & 0 & 0 & 0 & 0 & 0 & \dots \\ \hat{d}^2 V & 0 & c_1^2 \hat{d}^1 V & 0 & V & 1 & 0 & 0 & 0 & \dots \\ \hat{d}^3 V & 0 & c_1^2 \hat{d}^2 V & 0 & c_2^2 \hat{d}^1 V & 0 & V & 1 & 0 & \dots \\ \vdots & \vdots & \vdots & \vdots & \vdots & \vdots & \vdots & \vdots & \ddots & \ddots \end{pmatrix} \begin{pmatrix} g_\alpha \\ g_\beta \\ \hat{d}g_\alpha \\ \hat{d}g_\beta \\ \vdots \end{pmatrix}, \quad (29)$$

where  $\hat{d}^n = (d^n)/(dt^n)$  and  $c_m^n = n!/((n-m)!m!)$ .

This matrix is composed of a series of linearly independent column-vectors (when  $V(t) \neq 0$ ), and is thus invertible. Note that this matrix is a representation of the inverse of the extraction operator  $\hat{E}_x$ .

However, because in practice, successive derivatives of the  $V_m$  are prone to huge errors, we consider the following first-order approximation of the extraction operator:

$$\begin{pmatrix} \hat{V} \\ \hat{V} \end{pmatrix} = \begin{pmatrix} V & 1 \\ \hat{V} & 0 \end{pmatrix} \begin{pmatrix} g_\alpha \\ g_\beta \end{pmatrix}. \quad (30)$$

Inverting, we obtain:

$$\begin{pmatrix} g_\alpha \\ g_\beta \end{pmatrix} = \frac{1}{\hat{V}} \begin{pmatrix} 0 & 1 \\ \hat{V} & -V \end{pmatrix} \begin{pmatrix} \hat{V} \\ \hat{V} \end{pmatrix}, \quad (31)$$

when  $\hat{V} \neq 0$ . A finite difference first-order approximation of the last equation gives the following expressions

$$\begin{cases} g_\alpha(t+2\Delta t) = \frac{d}{dt} \ln(\hat{V}) \approx \frac{1}{\Delta t} \ln \left[ \frac{V(t+2\Delta t) - V(t+\Delta t)}{V(t+\Delta t) - V(t)} \right] \\ g_\beta(t+2\Delta t) = \hat{V} - g_\alpha V \approx \frac{V(t+2\Delta t) - V(t)e^{g_\alpha(t+2\Delta t)\Delta t}}{e^{g_\alpha(t+2\Delta t)\Delta t} - 1} \end{cases}. \quad (32)$$

Note that the values of  $t$  for which  $\hat{V} = 0$  are singular points of the first-order approximation of the extraction operator. Such singular points are due to the approximation of the extraction operator and vary with the order of the approximation. For example,

$$\bar{g}_\alpha = \frac{\hat{V}}{V} = \frac{(-1/C) \sum_{n=1}^N \hat{\Gamma}_n(t) [f(n\Delta) + g(n\Delta) + g_L] V + (1/C) \sum_{n=1}^N \hat{\Gamma}_n(t) [E_e f(n\Delta) + E_i g(n\Delta) + g_L E_L]}{- (1/C) \sum_{n=1}^N \Gamma_n(t) [f(n\Delta) + g(n\Delta) + g_L] V + (1/C) \sum_{n=1}^N \Gamma_n(t) [E_e f(n\Delta) + E_i g(n\Delta) + g_L E_L]}, \quad (38)$$

at the second order, the approximation of the extraction operator is given by:

$$\begin{pmatrix} g_\alpha \\ g_\beta \\ \ddot{g}_\alpha \\ \ddot{g}_\beta \end{pmatrix} = \frac{1}{\lambda} \begin{pmatrix} 0 & 0 & -3\ddot{V} & 2\dot{V} \\ \lambda & 0 & -3\dot{V}\ddot{V} & 2V\dot{V} \\ 0 & 0 & -\ddot{V} & \dot{V} \\ 0 & \lambda & -3\dot{V}\ddot{V} + V\ddot{V} & 2\dot{V}^2 - V\ddot{V} \end{pmatrix} \begin{pmatrix} \dot{V} \\ \ddot{V} \\ \ddot{V} \\ V \end{pmatrix}, \quad (33)$$

where  $\lambda = 3\ddot{V}^2 - 2\dot{V}\ddot{V}$ , and the singular points at second-order are those which obey  $3\ddot{V}^2 = 2\dot{V}\ddot{V}$  and not  $\dot{V} = 0$ . In this paper, we have only considered the first-order approximation because it is very difficult to accurately estimate with finite differences  $\ddot{V}$  and  $V$ . Nevertheless, if it was possible to have a precise algorithm to estimate these quantities, one could reduce the sampling rate of the voltage because the conductances could then be approximated by a linear time variation, which would be a significant gain. Note that to obtain a good first-order approximation, the sampling time must be sufficiently small so that the conductances can be considered constant over the interval.

## Appendix B. Analytic solution of extracted $g_\alpha$ and $g_\beta$

Because the extraction algorithm presented here is the inverse of the algorithm giving an exact solution of the standard RC-circuit

membrane model (see Eqs. (2) and (3)) for digitized conductances, it necessarily generates a third type of singular point which does not come from the first-order approximation of the extraction operator  $\hat{E}_{ex}$  (this happens when  $\hat{V} = 0$ ). In this appendix, we show how the digitization of the conductances can affect the results of the extraction of  $g_\alpha$  and  $g_\beta$  within this first-order approximation.

Let us assume that the conductances vary according to

$$\begin{cases} g_e(t) = f(t) \\ g_i(t) = g(t) \end{cases}, \quad (34)$$

which is sampled at a frequency  $f_e$ . The digitized conductances are then given by:

$$\begin{cases} \bar{g}_e(t) = \sum_{n=1}^N \Gamma_n(t) f(n\Delta) \\ \bar{g}_i(t) = \sum_{i=1}^N \Gamma_n(t) g(n\Delta) \end{cases}, \quad (35)$$

where  $\Delta = 1/f_e$  and  $\Gamma_n(t) = H(t - n\Delta)[1 - H(t - (n+1)\Delta)]$ . It follows that the values of digitized preconductances (see Eq. (3)) are given by:

$$\begin{cases} \bar{g}_\alpha(t) = -\frac{1}{C} \sum_{n=1}^N \Gamma_n(t) [f(n\Delta) + g(n\Delta) + g_L] \\ \bar{g}_\beta(t) = \frac{1}{C} \sum_{n=1}^N \Gamma_n(t) [E_e f(n\Delta) + E_i g(n\Delta) + g_L E_L] \end{cases}. \quad (36)$$

Thus,  $\hat{V}$  (see Eq. (2)) is given by:

$$\hat{V} = -\frac{1}{C} \sum_{n=1}^N \Gamma_n(t) [f(n\Delta) + g(n\Delta) + g_L] V + \frac{1}{C} \sum_{n=1}^N \Gamma_n(t) [E_e f(n\Delta) + E_i g(n\Delta) + g_L E_L]. \quad (37)$$

According to the first-order approximation of the extraction operator, we obtain the following expressions:

and

$$\bar{g}_\beta = \hat{V} - \bar{g}_\alpha V, \quad (39)$$

where  $\bar{g}_\alpha$  and  $\bar{g}_\beta$  are respectively the approximations of  $g_\alpha$  and  $g_\beta$ . We obtain:

$$\hat{\Gamma}_n(t) = \delta(t - n\Delta) [1 - H(t - (n+1)\Delta)] - H(t - n\Delta) \delta(t - (n+1)\Delta), \quad (40)$$

where Dirac delta functions will appear in the values of  $\bar{g}_\alpha$  and  $\bar{g}_\beta$ .

Because in this paper, the extraction algorithm is a finite difference approximation of

$$\bar{g}_\alpha = \frac{\hat{V}}{V},$$

singularities will appear at each numeric variation of the conductances.

Note that to approximate  $dg_\alpha/dt$  with finite differences at first order by assuming  $dg_\alpha/dt \approx \Delta g_\alpha/\Delta t$ , it is necessary that the sampling time interval is sufficiently long so that the Dirac delta functions caused by the digitization of the conductances are insignificant. However, in the extraction of preconductances we have to assume the opposite, namely that the time interval must be very small so that preconductances can be considered constant in the interval. In such a case, there will be strong discontinuous

jumps of preconductances, which will cause singularities. The latter criterion implies that we cannot approximate  $dg_{\alpha}/dt$  with finite differences (except when  $dg_{\alpha}/dt \approx 0$ ) without generating singularities (see Fig. 2). This is another reason why the voltage  $V$  must be sampled at a frequency greater than that of conductances, because the oversampled  $V$  allows to extract conductances in regions where no singularity appear (see Fig. 5).

### Appendix C. Approximation order of the voltage and preconductances

In this appendix, we show that if the error on preconductances is of first-order, then the error on voltage is second order. To simplify, we consider a time interval  $\Delta t$  starting at  $t=0$ , which leads to:

$$\begin{cases} g_{\alpha}(t) = a_0 + O(t) \\ g_{\beta}(t) = b_0 + O(t) \end{cases}, \quad (41)$$

where the term  $O(t)$  tends to 0 as  $t$  when  $t \rightarrow 0$ . It follows that

$$z = \exp\left(\int_0^t g_{\alpha}(\tau) d\tau\right) = \exp(a_0 t + O(t^2)), \quad (42)$$

such that the voltage must follow the following law (see Eq. (8)):

$$V(t) = e^{(a_0 t + O(t^2))} \left[ V(0) + \int_0^t (b_0 + O(\tau)) e^{-(a_0 \tau + O(\tau^2))} d\tau \right]. \quad (43)$$

Because  $e^{(a_0 t + O(t^2))} = e^{a_0 t} (1 + O(t^2))$ , we obtain:

$$V(t) = V(0) e^{a_0 t} + \frac{b_0}{a_0} (e^{a_0 t} - 1) e^{a_0 t} + O(t^2). \quad (44)$$

### References

Azouz R, Gray C. Cellular mechanisms contributing to response variability of cortical neurons in vivo. *J Neurosci* 1999;19:2209–23.

- Borg-Graham LJ, Monier C, Frégnac Y. Visual input evokes transient and strong shunting inhibition in visual cortical neurons. *Nature* 1998;393:369–73.
- Destexhe A, Rudolph M, Paré D. The high-conductance state of neocortical neurons in vivo. *Nat Rev Neurosci* 2003;4:739–51.
- Hines ML, Carnevale NT. The NEURON simulation environment. *Neural Comput* 1997;9:1179–209.
- Monier C, Fournier J, Frégnac Y. In vitro and in vivo measures of evoked excitatory and inhibitory conductance dynamics in sensory cortices. *J Neurosci Methods* 2008;169:323–65.
- Paré D, Shink E, Gaudreau H, Destexhe A, Lang EJ. Impact of spontaneous synaptic activity on the resting properties of cat neocortical neurons in vivo. *J Neurophysiol* 1998;79:1450–60.
- Piwkowska Z, Pospischil M, Brette R, Sliwa J, Rudolph-Lilith M, Bal T, et al. Characterizing synaptic conductance fluctuations in cortical neurons and their influence on spike generation. *J Neurosci Methods* 2008;169:302–22.
- Pospischil M, Piwkowska Z, Bal T, Destexhe A. Extracting synaptic conductances from single membrane potential traces. *Neuroscience* 2009a;158:545–52.
- Pospischil M, Piwkowska Z, Bal T, Destexhe A. Characterizing neuronal activity by describing the membrane potential as a stochastic process. *J Physiol Paris* 2009b;103:98–106.
- Robinson HP, Kawai N. Injection of digitally synthesized synaptic conductance transients to measure the integrative properties of neurons. *J Neurosci Methods* 1993;49:157–65.
- Rössler OE. An equation for continuous chaos. *Phys Lett A* 1976;57:397–9.
- Rudin W. Principles of mathematical analysis. 3rd ed. New York: McGraw-Hill; 1976.
- Rudolph M, Piwkowska Z, Badoual M, Bal T, Destexhe A. A method to estimate synaptic conductances from membrane potential fluctuations. *J Neurophysiol* 2004;91:2884–96.
- Rudolph M, Pospischil M, Timofeev I, Destexhe A. Inhibition controls action potential generation in awake and sleeping cat cortex. *J Neurosci* 2007;27:5280–90.
- Sadoc G, Le Masson G, Foutry B, Le Franc Y, Piwkowska Z, Destexhe A, et al. Recreating in vivo-like activity and investigating the signal transfer capabilities of neurons: dynamic-clamp applications using real-time NEURON. In: Destexhe A, Bal T, editors. *Dynamic-clamp: from principles to applications*. New York: Springer; 2009. p. 287–320.
- Sharp AA, O'Neil MB, Abbott LF, Marder E. Dynamic clamp: computer-generated conductances in real neurons. *J Neurophysiol* 1993;69:992–5.
- Wehr M, Zador AM. Balanced inhibition underlies tuning and sharpens spike timing in auditory cortex. *Nature* 2003;426:442–6.
- Wilent W, Contreras D. Dynamics of excitation and inhibition underlying stimulus selectivity in rat somatosensory cortex. *Nat Neurosci* 2005;8:1364–70.